Paolo Dario
Giorgio Buttazzo
Centro "E. Piaggio"
University of Pisa
Pisa, Italy

An Anthropomorphic Robot Finger for Investigating Artificial Tactile Perception

Abstract

In this paper the design, implementation, and testing of an artificial tactile sensing system incorporating an articulated robot finger are presented. It was our primary aim in this work to set up the hardware and software tools necessary for investigating basic issues in artificial tactile perception.

In the first part of the paper the criteria followed in the design of the robot finger and of its motor and sensory components are outlined.

The second part of the paper deals with the problem of defining a hierarchical architecture for the control of the exploratory finger. In this context, particular attention is devoted to the description of a set of tactile subroutines that are intended to replicate some of the basic sensory motor sequences adopted by humans for tactile exploration. The main features of the high-level planner, which is supposed to supervise the execution of those tactile primitives, are also discussed.

Finally, experimental results that demonstrate the capability of the robotic system of executing the previously defined tactile subroutines and of extracting specific object features are presented.

1. Introduction

The human hand is not only a remarkable tool capable of performing sophisticated prehensile functions, but it is also the true organ of the sense of touch (Kapandji 1970).

Most of the proposed theoretical analyses and practical realizations in the field of artificial hands for robots and prostheses have so far privileged the prehensile function of the hand (Okada and Tsuchiya 1977; Salisbury and Craig 1982; Jacobsen et al. 1984a), an approach justified by the fundamental importance and practical utility of prehension. However, investigating the function of the hand as a sensitive and accurate sensory receptor might also deserve some attention, both for its possible practical applications in advanced robotics and for the opportunities it offers in the study of artificial cognitive processes (Hillis 1981; Bajcsy 1984; Dario et al. 1985; Brock and Chiu 1985).

It is our aim to address the problem of replicating human tactile perceptual functions and to propose a simplified, experimental setup for testing some hypotheses on the structure of sophisticated artificial tactile sensing systems.

Because the accurate sensory motor control of exploratory acts forms the basis of any tactile perceptual strategy, the artificial environment we have designed is intended for investigating and, we hope, reproducing the basic motor paradigms necessary for tactile exploration. In this context, we adopted a practical perceptual approach based on the use of a single exploratory finger.

A single-finger scenario has been already proposed and partly implemented by Hillis (1981) and Bajcsy (1984) for the study of tactile exploration. However, those investigators neither considered in depth the fundamental problem of finger sensory motor control during tactile exploration, nor could they exploit the potential of a truly skinlike tactile sensor.

The first objective of our investigation was to design and construct a robot finger equipped with internal and external sensors and to address the problem of defining and executing a sequence of simple exploratory tactile procedures ("tactile subroutines"), each aimed at extracting a specific feature from the explored ob-

This work was partly supported by the Italian Ministry of Education (MPI 40%) and by NATO Scientific Affairs Division (Grant C.R.G. 85/224).

The International Journal of Robotics Research,
Vol. 6, No. 3, Fall 1987,

Fig. 1. The overall architecture of the tactile sensing system.

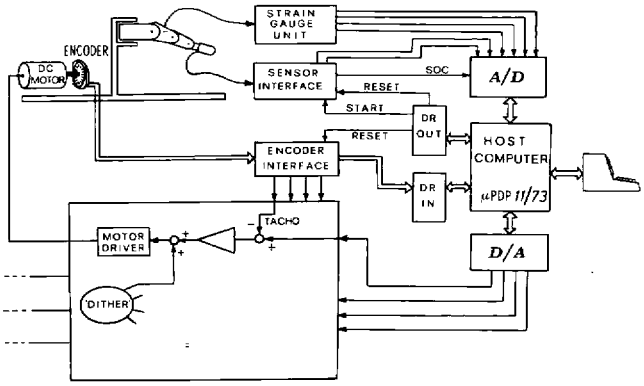

Fig. 2. The anthropomorphic four-degree-of-freedom exploratory finger.

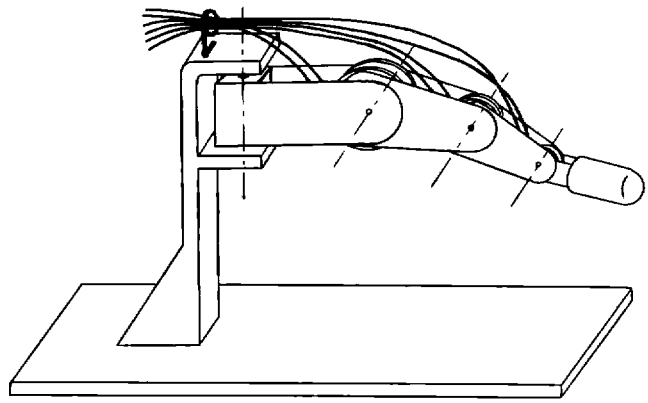

ject. The robot finger we have designed incorporates internal force and position sensors as well as exteroceptive, skinlike tactile sensors. It is intended to mimic the role of the human index finger as it explores objects lying on a table. In the scenario we have devised, the "table" actually consists of a sensorized static platform (not described here) that ideally replicates some functions of the palm of the hand (Dario et al. 1986).

The overall architecture of the sensorized setup we have developed is illustrated in Fig. 1.

In this paper the design and construction of the sensory and motor components of the anthropomorphic finger are discussed. A description of the software tools that implement the control strategies devised for tactile exploration is also given. Finally, some results obtained during experiments aimed at simulating simple tactile subroutines are presented.

2. Finger Design

The fundamental role of a finger during object exploration is to establish and control the contact between the fingerpad tactile receptors and the object.

In the context of our bionic approach to the study of artificial tactile perception, we have designed an anthropomorphic, four-degree-of-freedom exploratory finger, which is intended to be eventually connected to a multi-degree-of-freedom manipulator in order to become capable of following complex object surfaces (Bicchi 1984). In the present study, however, the finger is rigidly mounted on a fixture, as shown in Fig. 2. This configuration quite severely limits the exploratory capabilities of the finger; nevertheless, finger dexterity is sufficient to investigate fundamental problems associated with simple tactile procedures.

The finger is composed of four rigid links connected by hinge joints. The two-degree-of-freedom articulation of the proximal phalanx of the human fingers is reproduced by two separate joints with perpendicular axes.

The first design problem we have encountered was the choice of an appropriate actuation technique to drive the phalanges of the finger. Among various possible solutions (Okada and Tsuchiya 1977; Abramowitz et al. 1983; Salisbury 1984a; Jacobsen et al. 1984b; Nakano et al. 1984; Bridgestone 1985), we have elected to use dc servomotors as actuators and plastic-coated, stainless steel tendons routed through flexible and incompressible sheaths as the means to transmit power to the finger joints.

The cable-and-sheath configuration is simple and lightweight. Moreover, it substantially reduces the control complexity associated with cable-and-idle-pulley configurations, which determine the interdependence of joint motions (Salisbury 1984a).

We have attempted to reduce the friction effects caused by the tendons passing through the conduits by including those effects in the force control loop and by superimposing a "dither" vibration to the motor signal, which will be described later.

In the adopted configuration one dc motor actuates each joint through a pair of opposed tendons that are pretensioned to half the maximum required tension in

Fig. 3. A scheme of the cable-and-sheath arrangement used to drive each finger joint. The single-loop tendon consists actually of two pieces of stainless steel cable virtually joined at each pulley (see particular).

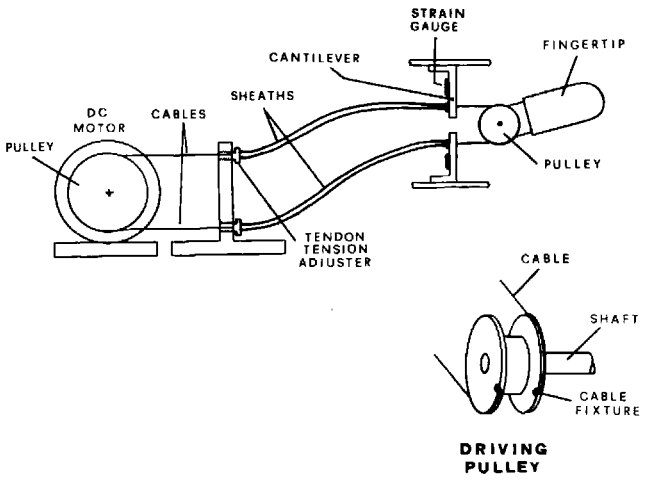

Fig. 4. View of the four dc motors driving finger tendons and of the optical encoders monitoring joint position and velocity.

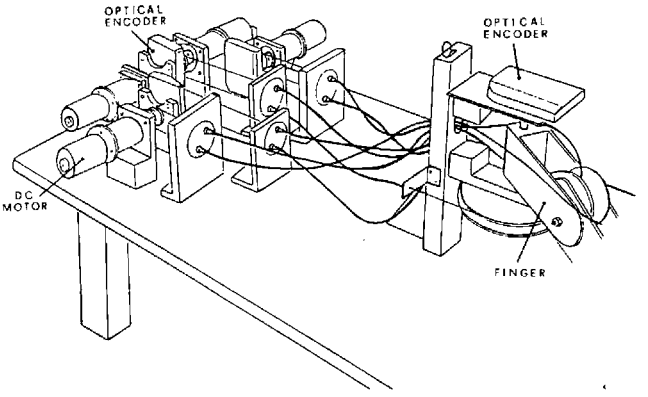

order to avoid slackening of one of the tendons during high force exertion.

A schematic diagram of the cable arrangement used to power each joint is shown in Fig. 3.

Joint position and velocity are detected by incremental encoders located (with the exception of the proximal joint) coaxially with the driving motors, as illustrated in Fig. 4.

Joint torques are measured by tendon tension sensors, consisting of cantilevers, instrumented with foil strain gauges, and located at the outlet of the conduits guiding the drive cables. The structure of the links, made of flat aluminum sections, and the disposition of the tendon tension sensors are depicted in Fig. 5.

The distal phalanx is equipped with a skinlike, ferroelectric polymer-based tactile sensor.

Link dimensions are not exactly anthropomorphic. We have elected to proportion each link in order to maximize the rectilinear excursion of the tactile sensor and to achieve optimal working conditions for exploratory tasks. From numerical calculations of the condition number of the Jacobian matrix for different proportionings of link lengths (Salisbury and Craig 1982), we determined that a configuration with $L_2 = L_3$ ensures optimal workspace quality. Accordingly, the finger link lengths were chosen to be $L_1 = 92$ mm, $L_2 = 61$ mm, and $L_3 = 61$ mm.

A side view of the actual finger workspace—i.e., the locus of points that can be reached by the fingertip tactile sensor—is shown in Fig. 6.

The mechanical proportioning of the finger was based on the assumption, appropriate for tactile exploration, that the fingertip should be capable of exerting a contact force of about 10 N (overload 30 N) and of moving at a maximum speed of 10 cm/s.

3. Sensors

The accurate, simultaneous control of contact force and position is fundamental during tactile exploration.

Obviously, force and position control requires the use of appropriate sensing means. In this section we present some general considerations on force and position sensing; then we discuss the features of the specific sensors in the exploratory finger.

The problem of force sensing for robot control has been addressed by many investigators, and various possible approaches have been identified (Shimano 1978). Among possible sensing techniques, joint torque sensing is probably most appropriate when high-speed operation is important, as with industrial robot manipulators (Wu 1985). Tactile arrays located on the finger surfaces contacting the explored object, or contact resolving fingertip sensors (Brock and Chiu 1985), seem more suitable for the control of low-speed, grasping, and exploratory tasks.

In principle, both tactile and contact-resolving sensors have the advantage of sensitivity and specificity in measuring contact force. However, they also have disadvantages. For instance, presently available tactile

Fig. 5. The structure of the exploratory finger, incorporating strain-gauge-based tendon tension sensors.

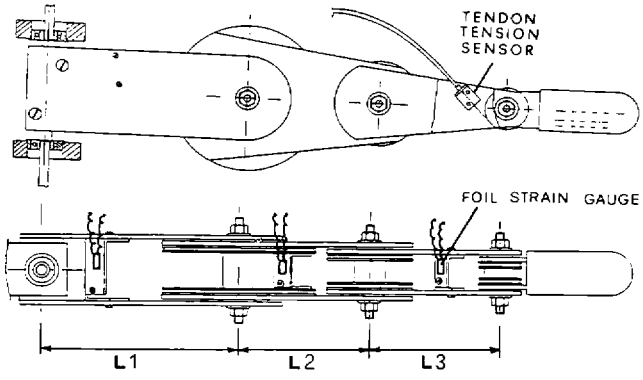

Fig. 6. Finger workspace (side view). The areas covered by the fingertip for extreme link positionings are shown along with a view of the 80 × 80 × 100 mm³ parallelepiped block that the finger is supposed to be fully capable of exploring. The shaded area is not practically usable for exploratory purposes.

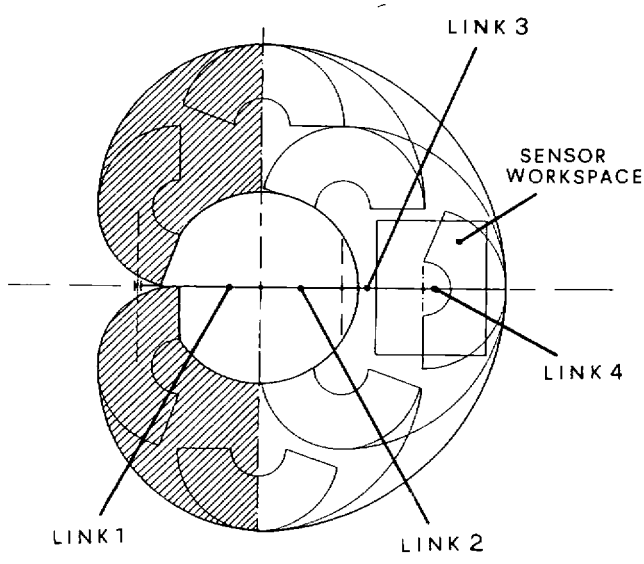

arrays lack accuracy and repeatability, and they have finite spatial resolution. Alternatively, a fingertip contact-resolving sensor can detect only the resultant of the contact forces acting on the fingertip, not their distribution: Thus, two or more contacts exerting forces could not be resolved uniquely. Furthermore, neither tactile nor fingertip contact sensors are suitable for controlling finger stiffness during exploration.

Based on all of these considerations, we elected to provide the exploratory finger with a force sensing system incorporating a set of different sensors with essentially separate functions: Fingertip skinlike tactile sensors are dedicated to exteroceptive sensing, and strain gauge devices measure tendon tensions (and, consequently, joint torques).

In the present version of the robot finger, the contact forces acting at the fingertip and at the other phalanges, as well as finger stiffness, are controlled only through the joint torque sensors. A version of the finger currently under development in our laboratory will also incorporate a new contact-resolving fingertip sensor conceptually similar to the one proposed by Salisbury (1984b). A contact-resolving fingertip tactile sensor is capable per se of some degree of exteroceptive sensing, since it can perceive some features of the local environment surface (Brock and Chiu 1985). However, in our present finger a thorough description of the geometrical and physical features of the object is obtained primarily through the fingertip tactile sensor array, which, like the human skin, possesses multiple sensing capabilities (Dario et al. 1985).

Joint position and velocity are monitored through optical incremental encoders, whose signal is used for servoing the dc motors. However, joint position signals are also processed at high control level in order to reconstruct the succession of contact points (as detected by the tactile sensors) and to infer the shape of the surface of the explored object.

The features of each sensing system equipping the robot finger are further discussed in the next sections.

3.1. Tendon Tension Sensors

A strain-gauge-based mechanism, schematically shown in Fig. 3, measures tendon tension by detecting the compressive force acting on each sheath of the circuit that transmits power from the motor to the joint.

Since each joint is powered by two counteracting, pretensioned tendons, a differential measurement of cable tension is possible by connecting in a single Wheatstone half-bridge the strain gauges that instrument two cantilever beams. Moreover, since sheath compression is measured at the outlet of each cable, it is possible to include the major sources of friction in each driving circuit (motor brushes, gears, cable and sheath) into a force control loop. Additional advantageous characteristics of this sensing arrangement are the independence of tendon tension measurement on

initial pretensioning, the doubling of sensor sensitivity, and the inherent temperature compensation.

3.2. Joint Rotation Sensors

The position and velocity of each finger joint are monitored by incremental optical encoders, which have the twofold advantage over potentiometers of introducing negligible friction and reducing computation time by presenting digital data to the control computer.

Directly measuring joint rotation at the joint axis would be desirable to reduce the influence of backlash in the power transmission chain (Jacobsen et al. 1986). However, since miniature encoders are not easily available, we mounted commercial encoders coaxially with the motor shafts (with the exception of the encoder monitoring the rotation of the proximal phalanx around the vertical axis, where space constraints are not too serious and inertial constraints are nonexistent).

A purposely designed interface, shown in Fig. 7, conditions the signals generated by each encoder and outputs TTL signals proportional to the absolute values of joint rotation angles to the 16-bit parallel interface of the DEC MicroPDP-11/73 that controls the finger. The interface also delivers analog signals proportional to joint velocities to the motor drive unit.

An automatic procedure, exploiting the one-pulse-per-rotation output from each encoder, has been devised to guarantee absolute finger position at initialization.

3.3. Tactile Sensor

The main goal of the fingertip tactile sensor is to provide the upper-level hierarchies of the control system with useful exteroceptive data to describe as thoroughly as possible the physical properties of the explored object. Accordingly, the tactile sensor we have incorporated in the fingertip is designed to extract, in

Fig. 7. Scheme of the encoder interface for position and velocity control.

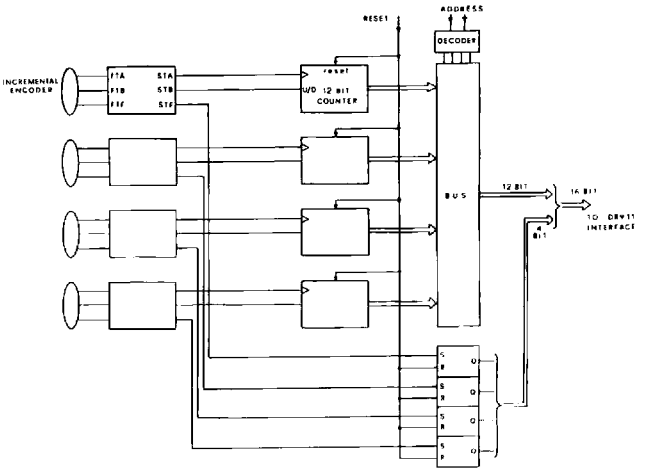

combination with appropriate motor acts, significant features from the object.

As described in other papers (Dario et al. 1984a; Dario and De Rossi 1985), our skinlike sensor is based on the technology of ferroelectric polymers and includes a deep ("dermal") layer and a superficial ("epidermal") layer having different sensing site disposition and spatial density. The two sensing films are separated by a compliant rubber layer.

The dermal layer, capable of providing quasi-static response to force signals, is intended to mimic the role of the slowly adapting (SA) receptors of the human skin, which are sensitive to the tiny spatial features of the indenting object (Phillips and Johnson 1981). The epidermal layer includes a few sensing sites concentrated in a small area (the "tactile fovea") and particularly sensitive, like the quickly adapting (QA) skin receptors, to dynamic contact stimuli.

As shown schematically in Fig. 8, the fingertip is cylindrical (diameter 21 mm) with a hemispherical tip (that, in the present implementation, is not sensorized).

The dermal sensor comprises 35 sensing sites arranged in a matrix of seven parallel rows, each including five elements, and oriented along the length of the finger (see Fig. 31). Sensing site disposition is determined by individual pin electrodes (diameter 2.5 mm) inserted radially (spacing 5 mm) in the fingertip frame, made out of PMMA. Microminiature coaxial cables are soldered to each electrode inside the fingertip and connected to a purposely developed prepro-

Fig. 8. The sensorized fingertip incorporating dermal and epidermal tactile sensors and a resistive heating layer.

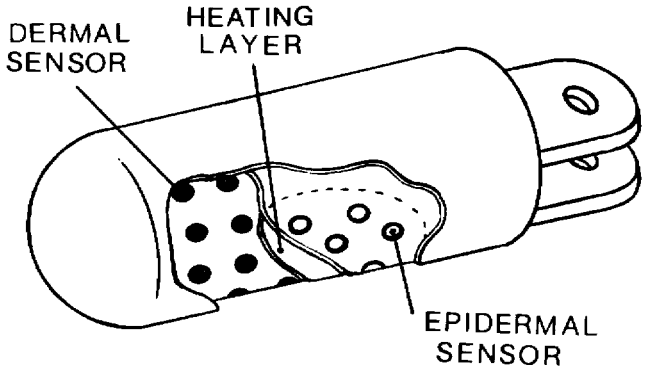

cessing electronics, presently located at the external surface of the finger links. Much denser sensor arrangements are possible. A new version of the fingertip sensor already built incorporates 128 sensing sites (diameter 1.5 mm, center-to-center spacing 2.5 mm) located on a much smaller sensing area, also including the hemispherical tip (Buttazzo et al. 1986).

The dermal sensor consists of a 110-micron-thick, flexible polyvinylidene fluoride (PVF2) film. The unmetallized bottom surface of the film is conformed to the cylindrical part of the fingertip and bonded to it with nonconductive epoxy. The outer surface of the PVF2 film is uniformly coated with a thin aluminum layer, which is then connected to the common shield of the miniature coaxial cables.

The dermal sensor is covered with a 1.5mm thick silicone rubber sheet, which supports the epidermal sensor. Such a sensor comprises a bottom heating layer (100 microns thick, 500 Ω resistance) of graphite-based resistive ink (Bardelli et al. 1983), and a 100 micron thick bilaminate PVF2 sensor incorporating a "fovea" of seven circular sensing sites (diameter 2.5mm) arranged in a hexagonal grid (center-to-center spacing 5mm).

Being rigidly backed, the dermal sensors operate predominantly in thickness mode, whereas the epidermal sensors are particularly sensitive to membrane strain (Dario et al. 1984b). As discussed in previous papers (Dario et al. 1984a), the signal detected by the two sensing layers, or their combination, allows us to measure various parameters of the explored object, such as space and time distribution of contact forces, surface roughness, material hardness, and thermal properties.

A feature of ferroelectric materials is their simultaneous sensitivity to mechanical and thermal stimuli. An additional characteristic of this class of materials is their inherent incapability of detecting truly static signals. A distinctive property of ferroelectric polymers is their excellent linearity and very large bandwidth (Sessler 1981).

A goal of our investigation was to devise appropriate working conditions for the tactile sensor in order to exploit the advantages of ferroelectric polymer materials and to reduce the effects of their drawbacks. This approach was pursued, as will be discussed in the following, by separating the functions of the different tactile sensors: In particular, though truly static force signals, essential for force control, are provided by the strain gauge tendon tension sensors, the fingertip receptors have the role of sensing predominantly dynamic signals, which is required by active touch exploration and which is suitable for piezoelectric sensors.

Nevertheless, since reading quasi-static variations of contact pressure may be important for the detection of object features (corners, edges, holes), we have also investigated the possibility of obtaining quasi-static signals from a matrix of ferroelectric polymer sensors.

Scanning a matrix of piezoelectric and pyroelectric sensors is a complex issue. We have devised a method that combines the advantages of charge amplification with the possibility of reducing the encumbrance of the electronic circuitry typical of multiplexing techniques (Basta 1985). In the following paragraphs, a brief description of the scanning technique we have implemented is given. A block diagram of the scanning and signal-amplifying electronic unit is shown in Fig. 9 for a subset of 16 sensors.

The 42 dermal and epidermal sensors are scanned sequentially by analog multiplexers whose output is delivered to a single charge amplifier. After each sensor reading, the feedback capacitor of the charge amplifier is reset so the same initial conditions are obtained each time a channel of the multiplexer is selected. Since this technique implies the "destruction" of the charge produced piezoelectrically or pyroelectrically by each sensor during the interval between two successive readings, only charge variations are measured. Therefore, the true force signal must be reconstructed from the voltage increments corresponding to charge variations.

Fig. 9. Block diagram of the processing unit designed for amplifying and reconstructing the charge signal generated by each element of the PVF2 tactile sensing matrix.

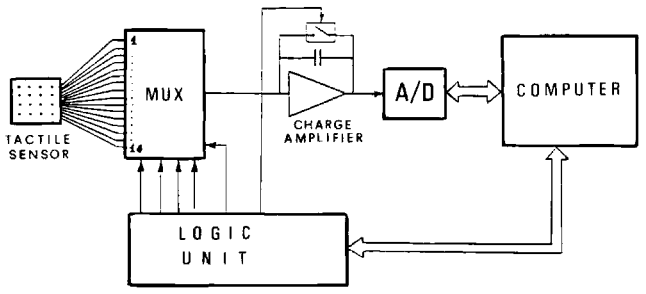

Fig. 10. Diagrams illustrating typical performances of the scanning electronic unit and of the algorithm that reconstructs the temporal variations of the force exerted on a sensing element of a ferroelectric polymer tactile sensor.

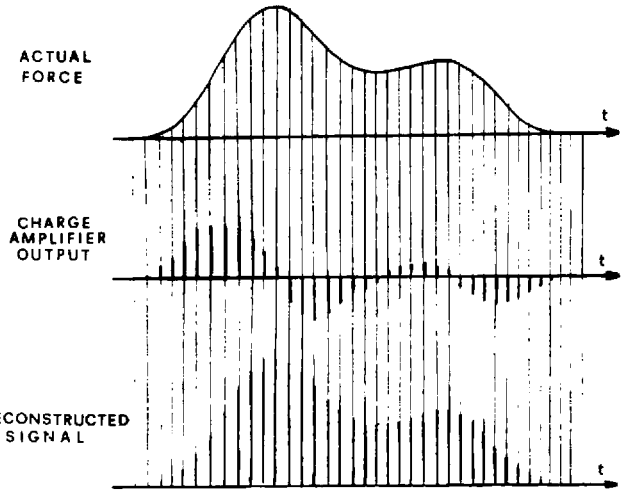

If T is the multiplexer scanning period (equal to the time required to process a single sensor reading) and N is the number of sensors in the array, each sensor will be read with a period equal to NT. Then, if $V_i(kNT)$ is the voltage obtained by the kth reading of the ith sensor, the force acting on the ith sensor at the instant $t_k = kNT$ will be

$$F_i(t_k) = h \sum_{j=0}^{k} V_i(jNT), \tag{1}$$

where h is the proportionality constant between the force and the voltage (in newtons per volt).

To exemplify this procedure, we show in Fig. 10 a variable-force signal acting on a sensor along with the voltage signals produced by the scanning circuit for the same sensor and with the reconstructed signal, obtained by summing the voltage increments.

A fundamental problem of the proposed method is the virtual reduction of the wide intrinsic bandwidth of the polymer sensor signal determined by the scanning procedure. The sensor reading rate depends on array sensor number and on computer scanning velocity.

From the sampling theorem we obtain

$$f_H < 1/2NT, \tag{2}$$

where f_H is the maximum frequency of the tactile signal.

In the present case, T includes the time required to transfer the charge generated by each sensor into the feedback capacitor (about 5 μs), the A/D conversion time (about 25 μs for the DEC ADV11-C converter we use), and the time required by the computer to process some assembler instructions: a total of about 40 μs. The bandwidth of the reconstructed signal, which depends on sensor number, can be calculated. The values of f_H corresponding to different sensor numbers are given in Table 1.

Obviously, processing time could be reduced and f_H could be increased if faster A/D converters were used.

A serious problem we encountered during the development of the matrix processing unit was the presence of offset levels at the output of the charge amplifier, even when no force was exerted on the sensors. Furthermore, the offset levels varied from sensor to sensor. This problem would have not been too serious if these voltage levels were stable in time. It would be possible to compensate the offset levels by reading and storing their initial values in a look-up table during the initialization phase. Unfortunately, initial levels are affected by different sources of noise, namely (a) high-frequency noise, (b) very low-frequency noise leading to random signal drift, and (c) disturbances from network voltage, which introduce a beat frequency between the network frequency and the circuit sampling frequency. These sources of noise (particularly the low-frequency drift) cause problems in signal reconstruction, the most serious being a large, variable drift.

The technique we devised to solve this problem consists of reading each sensor twice consecutively, with a time interval of about 40 μs between the two readings. The first reading provides a voltage value corresponding to the force variation that occurs in the interval between the previous (second) reading and the present reading (including noise), but the second read-

Table 1. Maximum Frequency Content of the Signal Reconstructed Through the Proposed Technique for Different Sensor Numbers (N).

N	f_H (Hz)
32	390
42	298
64	195
128	97
256	48

ing does not include any significant contribution from force variations [which we have assumed to be slower than the limit given by Eq. (2)].

Although this method reduces the upper limit of signal bandwidth to half the values reported in Table 1, it proved to be very effective in reducing signal drift to an acceptable level.

The signal is then reconstructed from the following simple algorithm:

```
FOR I = 1 TO N
⟨C(I) ← first reading⟩
⟨V(I) ← second reading⟩
R(I) = R(I) + C(I) − V(I)
NEXT I
```

where

$\mathbf{C}(I)$ = vector of the first readings,
$\mathbf{V}(I)$ = vector of the second readings,
$\mathbf{R}(I)$ = vector of the reconstructed signals.

Typical experimental results demonstrating the capability of the double-sensor-reading technique of improving the accuracy of signal reconstruction are reported in Fig. 11.

Fig. 11. Experimental results illustrating the typical behavior of a ferroelectric polymer tactile sensor upon imposition of a step force signal. The double-reading technique clearly improves the response of the PVF2 sensor compared with single reading.

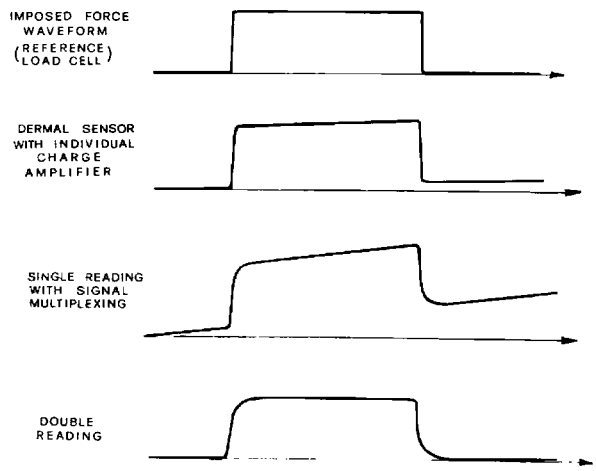

4. Sensor-Based Finger Control

Human tactile perception involves sophisticated sensory motor activities controlled by the central nervous system, whose hierarchical structure comprises different, closely interrelated, control levels (Albus 1981).

To approach the problem of replicating in an artificial system some of the processes unique to human tactile perception, we have considered the simplified, three-level control architecture illustrated in Fig. 12. At the bottom level of the control hierarchy, servo loops control finger joint positions and torques through feedbacks from internal sensors. The intermediate level has the capability of controlling autonomously the execution of tactile subroutines, whose sensory motor procedures have been learned and stored previously. The top hierarchical level should ideally reproduce the upper functions of the brain, including the capability of deciding tactile exploratory strategies, calling appropriate tactile subroutines, and processing sensory information to construct a model of the explored object. Through hypothesis verification procedures, the model would be compared with models already stored in a data base and either recognized or inserted as a new object in the same data base.

Investigating the features of the upper control level of this class of tactile perceptual systems is an open research field for artificial intelligence (A.I.) and, as suggested by Turing (1950), the most appropriate way to reproduce the rise of intelligence and abstract thought in an artificial system.

Although we shall present some preliminary considerations on the structure of the high-level controller, our attention is dedicated predominantly to investigating the possible features of the two lower levels of the control hierarchy depicted in Fig. 12. In particular, we

Fig. 12. Hierarchical control architecture for tactile exploration.

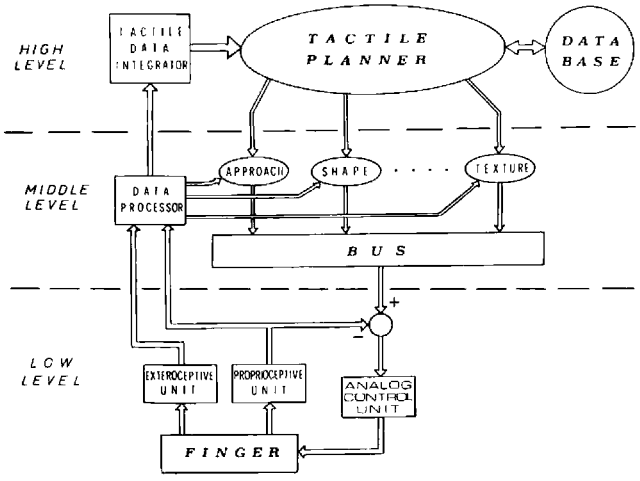

set up the hardware and software tools necessary to investigate and test appropriate sensory motor tactile exploratory subroutines and to store them at the intermediate control level.

The computational architecture implementing the control hierarchy of the proposed tactile system should be most obviously based on a distributed multiprocessor network (Goldwasser 1984; Kriegman et al. 1985). A possible configuration for such computer architecture would include a number of microprocessors for low-level finger motor control, a minicomputer (or an evolved microcomputer) for commanding tactile subroutines, and a supervising computer managing high-level control strategies through procedures typical of A.I.

In this context, the role of the supervisor would be fundamental, for instance, in solving possible ambiguities of the sensory data, either by comparing different sensory information or by deciding and commanding appropriate tactile operations to obtain new data and verify hypotheses. For instance, pressing the skinlike sensor on the explored object could help in some situations by determining a sort of "focusing" on the desired object feature and thus improving feature extraction. Alternatively, in other situations typical of a multisensory approach to object exploration, the finger could move the object in the field of view of an artificial vision system and facilitate object recognition.

For our current investigation, it is sufficient to use an evolved microcomputer, such as the DEC MicroPDP-11/73, to implement the control loops necessary to manage simple tactile exploratory primitives.

4.1. Low-Level Control System

As we have already pointed out, a control system for tactile exploration should guarantee that the fingertip sensor moves along the surface of an object and exerts simultaneously a controlled contact force in order to elicit tactile stimuli from the sensor. Hence, a fundamental feature of the controller is the ability to provide a hybrid (position-force) control of the joints (Salisbury 1980; Raibert and Craig 1981; Zhang and Paul 1985; Khatib 1985).

We have designed a hybrid control system specifically intended for tactile exploration. The features of this controller, discussed by Bicchi et al. (1985), will be described in detail in the next section.

The low-level control system we describe here is designed to execute the hybrid commands sent by the middle-level controller. A block diagram of the low-level control system is shown in Fig. 13, in which

$\mathbf{Q}$ = nominal joint position vector: $|Q_1, Q_2, Q_3, Q_4|^T$,
$\mathbf{T}$ = nominal joint torque vector: $|T_1, T_2, T_3, T_4|^T$,
$\mathbf{A}$ = actual joint position vector: $|A_1, A_2, A_3, A_4|^T$,
$\mathbf{G}$ = actual joint torque vector: $|G_1, G_2, G_3, G_4|^T$,

$\mathcal{C}$ = compliance matrix:

$$\begin{pmatrix} C_1 & 0 & 0 & 0 \\ 0 & C_2 & 0 & 0 \\ 0 & 0 & C_3 & 0 \\ 0 & 0 & 0 & C_4 \end{pmatrix},$$

U = hybrid signal,
S = sensor signal.

At this level the position and torque control of the device is accomplished in the joint space, where each joint can be controlled independently and directly.

The hybrid control law we use may be expressed in the form

$$U = \mathcal{C}(T - G) + (\mathcal{J} - \mathcal{C})(Q - A),$$

where $\mathcal{J}$ is the identity matrix.

The diagonal compliance matrix $\mathcal{C}$ controls the stiffness of the movements and acts as a balance factor

Fig. 13. Block diagram of the low-level control system.

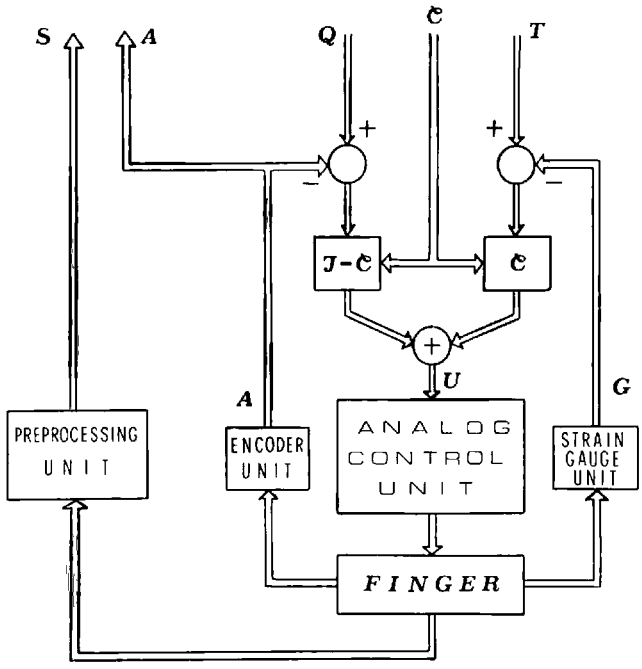

between the torque command and the position command. For each element of $\mathcal{C}$ the bounds $0 \leq C_i \leq 1$ hold. Hence for $\mathcal{C} = \mathcal{J}$ the finger has maximum compliance; for $\mathcal{C} = 0$, maximum stiffness.

Torque and position commands are mixed by software, so compliance can be controlled by the upper levels of the control system. The resultant hybrid command U is sent to an analog control unit, which drives the actuation system of the finger.

The signals detected by the exteroceptive tactile sensors are digitized and preprocessed in order to send the middle-level controller only signals significant for the specific tactile subroutine it is requested to execute. Most of such signal preprocessing, which in the present research stage is performed by the same computer, could be easily carried out by a dedicated microprocessor unit.

The analog unit implementing low-level control functions is illustrated in detail by the block diagram in Fig. 14, in which

J = motor's inertia,
B = motor's damping constant,
θ = rotated position of motor,
ω = rotated velocity of motor,

Fig. 14. Block diagram of the low-level servo loop.

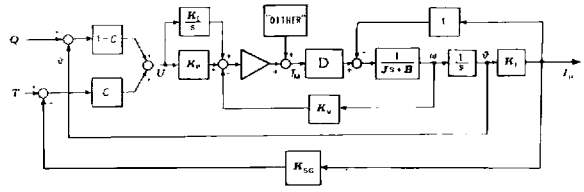

K_I = integral gain,
K_P = proportional gain,
K_E = finger structure elasticity,
K_V = velocity feedback gain,
K_{SG} = torque feedback gain,
D = descriptive function of friction effects.

The block "dither" indicates a generator of high-frequency vibration $f(\Omega t)$.

The output T_R represents the actual torque exerted by each joint. Force and position feedback loops have been also included, even if they are actually performed by software.

Moreover, the following equations hold for our control system:

$$U = \mathcal{C}(T - K_{SG}T_R) + (1 - \mathcal{C})(Q - \theta),$$
$$T_M = (K_P + K_I/S)U - Kv\omega + f(\Omega t),$$
$$T_R = \frac{K_E}{s}\frac{1}{Js + B}(T_M D - T_R) = \frac{K_E D}{Js^2 + Bs + K_E}T_M.$$

The friction introduced by the cable-and-sheath transmission determines a strong nonlinearity of the system whose stability is not always guaranteed.

An analysis carried out by the descriptive function method (see Appendix I) indicated the existence of a limit cycle (also verified experimentally) whose amplitude and frequency depend on the gain K_P and on the elasticity coefficient K_E. The high-frequency vibration (dither) in the action chain was introduced to solve this problem. This superimposed vibration drives the system to oscillate with a frequency that, being the system of the lowpass type, is easier to filter.

Figure 15A,B illustrates the effect of the dither technique on the signals measured by the joint torque sensors, by the PVF2 tactile sensor, and by a reference load cell that the fingertip was commanded to press. As the diagrams demonstrate, without any superimposed dither vibration all the signals are strongly dis-

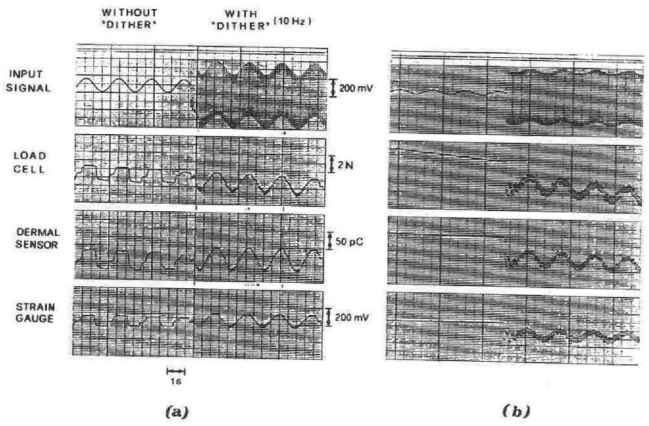

Fig. 15. Effects of the superimposition of a dither vibration on the finger command signal. The finger presses a calibrated load cell, whose signal is shown along with the outputs from the PVF2 dermal sensor and from a joint torque sensor. When a high-intensity command signal is imposed (A), the dither dramatically improves the faithfulness of finger response. For a low-intensity command signal (B), the finger starts moving only upon the application of a dither signal.

torted (A), and the system does not even respond to small-amplitude command signals (B). When a 10-Hz vibration is superimposed instead, sensor response becomes quite linear and appears even with small input signals.

This effect can be explained by observing that, in the presence of vibration, the cables are continually kept moving. Hence, the "stick and slip" effect, determined by the sudden variations of the resistant force resulting from the difference between static and dynamic friction coefficients, is eliminated.

Dither signal intensity and frequency can be properly adjusted to negligibly affect the signal detected by the tactile sensors.

To summarize: The signals that the low-level control system receives from the middle-level controller are Q, T, and $\mathcal{C}$. The signal originated from the tactile sensor is sent from the low-level controller to the middle level and then, after an appropriate signal preprocessing that depends on the tactile task, to the upper-level controller.

Moreover, force and position signals may also be fed back to the middle-level controller to perform special tactile subroutines (for instance, the measurement of material hardness).

4.2. Middle-Level Control System

The middle level has the role of managing the execution of the tactile subroutines selected by the high-level controller. Although many different "subroutines" could be considered, we have elected to investigate the following representative subroutines, which can be realized with the PVF2 skinlike tactile sensors we have fabricated: APPROACH, SHAPE, TEXTURE, HARDNESS, THERMAL.

We shall briefly describe the implementation of these subroutines, based on the assumption that the contact between the finger and an object always occurs at the sensorized fingertip level and involves both epidermal and dermal sensing layers.

The subroutine APPROACH manages finger motion until the fingertip touches the object. The approaching motion can be blind or guided by proximity sensing [for instance, by vision, pseudovision (Dario et al. 1986), infrared radiation, or optical or ultrasonic ranging].

Assuming that some approximate information is available to the high-level controller on the point of the object that the finger should initially touch, the coordinates of such a point (x, y, z) are sent to the middle-level controller, as shown in Fig. 16.

The high-level controller sets the value of T so that the finger exerts a small assigned contact force, and the value of $\mathcal{C}$ so that the finger deforms compliantly to avoid damaging the object and/or itself.

During the approaching motion the middle-level controller analyzes the signals from epidermal and dermal sensors (S), and from the strain gauge devices (G). If the signal detected by the epidermal sensors is negative in sign and larger than a given threshold, the controller infers that the finger is approaching a hot object. The temperature rise induced in the epidermal sensor by the radiant heat emitted by a hot object generates negative electric charge by the pyroelectric effect. A suitable algorithm, which provides "instinctive," fast reactions to potentially dangerous situations, immediately stops the motion and retracts the finger.

An additional dangerous situation can be managed by the subroutine APPROACH by exploiting the fast response and high sensitivity of the epidermal sensors, as well as the presence of higher-resolution dermal sensors underneath. When the fingertip touches a sharp object, the epidermal sensor membrane is stretched and produces a large positive signal by piezoelectric effect; at the same time the dermal sensors assess that the contact area is small. Since contact

Fig. 16. Block diagram of the subroutine APPROACH.

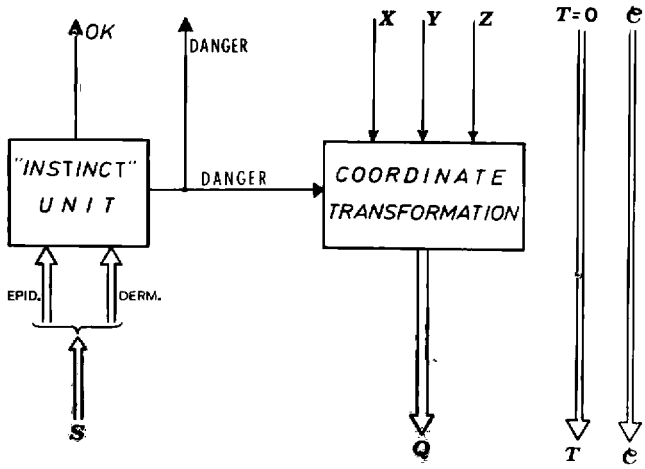

force is also small, the strain gauge unit is usually not sensitive enough to detect promptly a dangerous tear strain in the skin sensor. As before, the "danger" instruction stops and retracts the finger.

When encountering potentially dangerous hot or sharp objects, the finger's "instinctive" reaction avoids overheating or tearing the skin sensor.

The danger message is also sent to the high-level controller, which decides further strategies.

If no dangerous situation is detected at the cutaneous level by the tactile sensors the finger compliantly presses the object with a force T measured by the strain gauge tendon tension sensors. When the finger stops, the instinct unit sends the upper controller an O.K. message, authorizing it to command a new subroutine.

The subroutine SHAPE allows the finger to follow the surface of the object and to infer its three-dimensional shape by reconstructing the locus of the contact points.

The informative concept of SHAPE is to start object tactile exploration from a given position (for instance, the one the finger has reached at the end of APPROACH) without any a priori knowledge of the trajectory to follow. This is the distinctive feature that renders our approach to hybrid control different from other hybrid methods, whose application is based on the hypothesis that a position trajectory is already assigned in terms of base coordinates. In that case the assigned trajectory could be modified during its execution, if contact forces are detected, compatibly with the compliance specifications given in the appropriate reference frame (Paul 1981).

Instead, during tactile exploration the task is completely specified in the compliance reference frame. Because exploring a surface is a surface-driven task, the controller does not know the way the fingertip will go, but it knows that the path followed belongs to the surface of the explored object. Hence, the motion of the exploratory finger will be determined in real time by sensory feedback.

To implement these concepts, SHAPE first considers the common normal direction to the contact point between the fingertip and the object, and the tangent plane to the same point; then the finger is commanded to move a step along a direction belonging to the tangent plane and to exert simultaneously a given force against the object along the normal direction. Step length, step direction, and contact force intensity are decided by the high-level controller, also on the basis of other possible sensory data.

Force and position commands are therefore inherently consistent with the physical constraints imposed by the contact, at least compatibly with sensor imperfections (a tactile sensor array would require very high spatial resolution; a force-resolving fingertip would probably be an ideal solution).

A suitable fingertip sensor shape facilitates the unique determination of the contact point. The most appropriate shape of the fingertip would be spherical. However, since constructing a spherical fingertip sensor is quite difficult, we have adopted a cylindrical configuration. This configuration along with the limited finger dexterity severely reduces the generality of the surface that can be explored.

A schematic diagram illustrating the primitive SHAPE is given in Fig. 17.

The high-level controller sets the values of θ (the direction of motion in the plane tangent to the contact point), L (step length), F (contact force intensity), and $\mathcal{C}$. Fingertip sensor signals are processed in a coordinate transformation unit that considers only the dermal sensors and calculates from them the coordinates of the contact point in the base frame. The information relative to the coordinates of the contact point (P)

Fig. 17. Block diagram of the subroutine SHAPE.

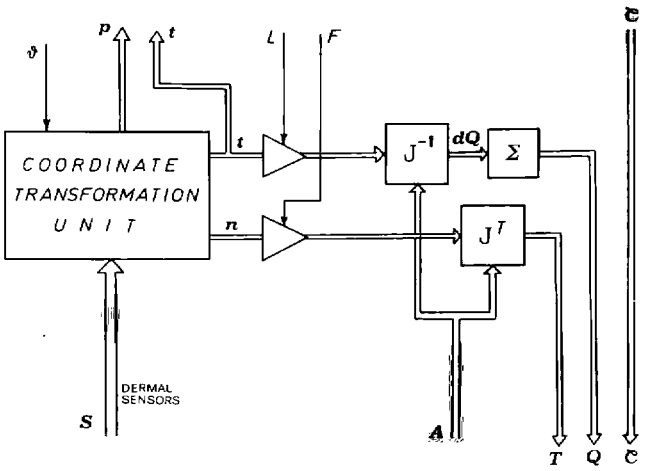

Fig. 18. Block diagram of the subroutine TEXTURE.

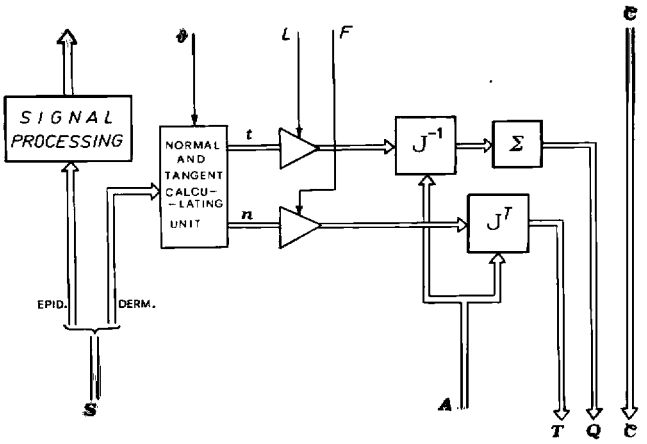

and to the tangent direction (t) are sent to the upper controller for the reconstruction of object shape.

The transformation unit also calculates normal (n) and tangent (t) directions in the fingertip frame. The tangent unit vector is multiplied by L, and the result is applied to the Jacobian inverse matrix, which provides the angular increments dQ of each joint. The sum of those increments is sent to the low-level controller as the nominal position command.

The normal unit vector is multiplied by F, and the result is applied to the Jacobian transpose matrix, providing the nominal torque command. Details of the computations required in the case of our four-degree-of-freedom finger are presented in Appendix II.

TEXTURE could be called and executed after the shape of the object has been reconstructed, or even before if the tactile exploration of the overall shape is not considered essential by the "tactile planner."

The aim of TEXTURE is to estimate the finish of parts of the object surface. This estimate is obtained by rubbing the fingertip sensor gently over the desired surface while exerting a predetermined, adjustable force on it, and by analyzing the signal elicited by this procedure in the sensitive, superficial epidermal sensors.

Since fine-texture details are better perceived by humans by exploring planar surfaces, the high-level controller could also decide a similar strategy for the finger.

The block diagram of TEXTURE in Fig. 18 shows that this tactile primitive is similar to SHAPE in the strategy adopted to track object surfaces, but differs from it in that the waveform detected by the PVF2 epidermal sensors is processed separately to derive possible significant signal features relative to local roughness.

Note that in SHAPE the "attention" of the high-level controller was focused on P and t (both derived from the signal detected by the dermal sensors); during TEXTURE the dermal sensor signal is processed only at low level without any "conscious" involvement of the upper hierarchies of the controller, and the attention of the controller is devoted only to the epidermal sensor signal.

A possible method of detecting surface features first involves highpass filtering the epidermal sensor signal to avoid the influence of possible slow variations of contact force and object temperature. Then the spectrum of the resulting signal can be analyzed in order to extract features useful to the high-level controller to classify and recognize different vibration patterns (Patterson and Nevill 1986).

The primitive HARDNESS is intended to provide the high-level controller with data relative to the elastic properties of the material out of which the object is made.

Although we can estimate the elastic modulus of the material by monitoring joint torque and fingertip position while the object is pressed, the composite PVF2 tactile sensor incorporated in the exploratory

Fig. 19. Block diagram of the subroutine HARDNESS.

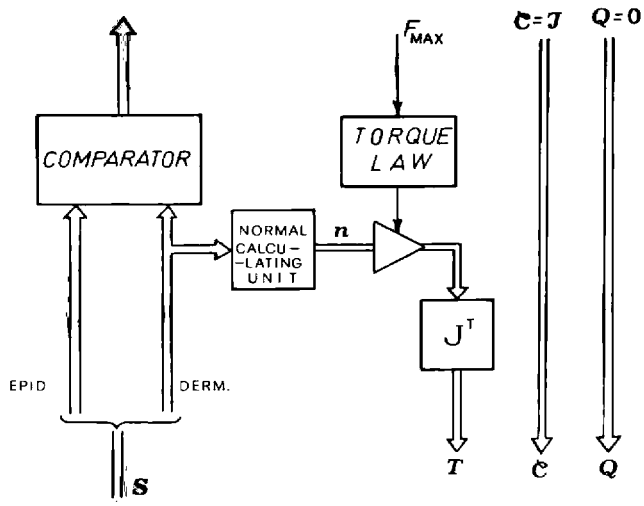

Fig. 20. Block diagram of the subroutine THERMAL.

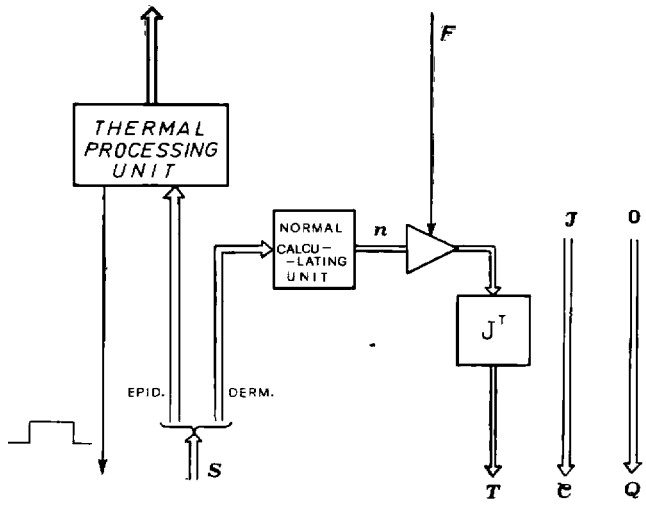

finger lets us calculate material hardness directly from the measurement of epidermal and dermal sensor signals. As we later show, the ratio between the output of the dermal sensing element pressed on the object and the output of the epidermal sensor immediately above give a relatively accurate figure of merit of material hardness, provided that the touched surface is flat.

According to the block diagram in Fig. 19, during HARDNESS the finger is commanded only through a torque law (for instance, sinusoidal), while remaining at a suitable (flat) location of the object surface.

The signal detected by the dermal sensors is used for controlling the direction along which the force is exerted. However, the signals from the epidermal and dermal sensors are also independently processed in order to calculate the figure of merit of material hardness, which allows the high-level controller to distinguish some different materials (for instance, rubbers with elastic moduli between that of foam and hard rubber).

THERMAL identifies different materials on the basis of their thermal properties. The method we follow develops the approach first proposed by Hillis (1981) and Harmon (1982), demonstrated in our laboratory (Bardelli et al. 1983; Dario et al. 1984b), and recently further investigated by Russell (1985) and Siegel et al. (1986). According to this approach, we can correlate the temperature variation, which is induced in the cutaneous tactile sensors by the heat flowing from a source within the sensor toward the object under examination, with the thermal diffusivity (during the temperature transient) or conductivity (at equilibrium) of the material of which the object is made.

To estimate material thermal properties, we stop the finger first in a position corresponding to a flat portion of the object surface; then the tactile fovea is pressed slightly on the object (and kept pressed), as indicated in Fig. 20. The signals measured by the dermal sensors are used, as in previous cases, to control the direction of contact force.

These preliminary operations are intended to reduce the influence of object shape differences and of thermal contact conditions on sensor reading.

After having established appropriate contact conditions, the "thermal processing unit" commands a power supply unit to produce a current pulse in order to heat the resistive graphite layer incorporated in the tactile sensor. The epidermal sensor monitors the temperature variations occurring at the finger–object interface during both the heating phase and the successive cooling phase when the power supply is turned off. We can estimate material thermal coefficients by considering the variation of the signal during transient phases, the largest pyroelectric signal detected by the

epidermal sensor, and the value of the epidermal signal after a given interval (typically a few seconds) from the trailing edge of the heating pulse.

Heating the fingertip sensor only after the object has been pressed avoids a piezoelectrically generated signal from interfering with the pyroelectric signal of interest. We have demonstrated experimentally that the sensitivity of the PVF2 sensor is high enough to allow it to distinguish not only metals from plastics but even, within each material class, different metals and plastics.

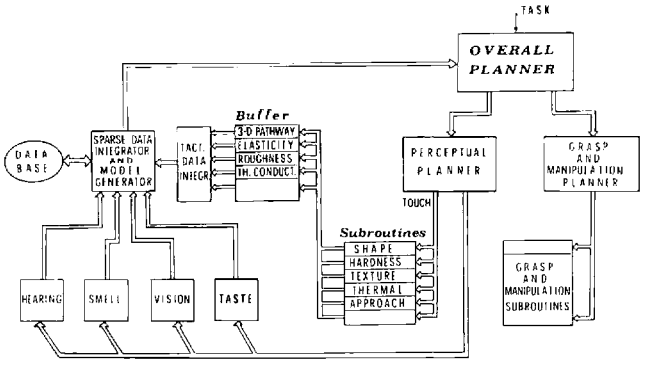

Fig. 21. Block diagram of a possible implementation of the high-level control system.

4.3. High-Level Control System

In this section we briefly discuss some of the desirable features that a high-level controller should incorporate to supervise the execution of the tactile primitives we have proposed.

Although most of the components of this control architecture have not yet been practically implemented, such an architecture represents the ideal frame for the artificial perceptual system we are currently investigating.

Referring to the scheme in Fig. 21, we can assume that a task requiring skilled manipulation (i.e., the assembly of randomly oriented known and unknown parts) is assigned by the top-level, decision-making centers of a hypothetical intelligent supervisor to the overall planner. The overall planner can decide and command either a purely grasping and manipulative strategy based on the existing knowledge of environment organization or a perceptual strategy intended to acquire sensory data to integrate such a knowledge basis.

First suppose that the overall planner needs to gather additional information to carry out the desired manipulative task. The perceptual planner will tentatively decide a sequence of exploratory actions, represented by the previously described tactile subroutines, and will also command other sensory systems to collect (either actively or passively) specific sensory data. Each sensory system is expected to be controlled by an independent processor.

Data collected during the execution of each tactile subroutine will be stored in a buffer as a sequence of information. Then bufferized data will be sent to a tactile data integrator, which will output a flow of synthetic information on the explored object. From the description of the three-dimensional pathway, the integrator could output high-level information on, say, the position, area, and depth of a hole or on the most significant frequency components of the signal produced by TEXTURE.

Additional synthetic data, generated by the other sensory processors, will be sent along with tactile data to the sparse sensory data integrator. Based on those data, the integrator will generate dynamically a model of the object, which will be compared, also dynamically, with models stored in a data base.

According to the result of such a comparison, the overall planner may decide on further strategies (for instance, further exploratory acts) to either recognize the object or classify it as new.

As already anticipated, the overall planner can also command manipulative tasks without the need for tactile exploration, if the data provided by other sensory systems are informative enough. However, if during the execution of grasping and manipulative subroutines a need arises for the refinement of available information on object features, the overall planner may decide specific exploratory tasks.

The execution of simple manipulative subroutines can also be commanded by the overall planner to render other sensory modalities more effective. For instance, an object could be rotated, after being grasped, in order to better visualize possible hidden features.

Finally, when the output from any tactile receptor exceeds a threshold value, that signal is assigned abso-

lute priority among those received by the overall planner. This "alarm" function has a role equivalent to that played by the nociceptors of the human skin.

5. Experimental

As a first step toward fully implementing the overall control architecture discussed in the previous sections, we have elected to investigate the practical realization of the proposed tactile subroutines. We shall now describe the implementation of each subroutine and the results obtained during preliminary experiments.

Each tactile subroutine consists of a main program written in BASIC-PLUS-2 and of subroutines written in MACRO-11, running on a DEC MicroPDP-11/73 computer.

Because no upper-level controller has actually been developed yet, each subroutine requires inputting from a terminal all the parameters that are expected to be provided in the final implementation of the system by such a high-level control unit.

5.1. APPROACH

This subroutine has been tested under the following experimental conditions: The tip of a laboratory soldering iron was located within the working volume of the finger. The base frame coordinates (x, y, z) of the tip were input to the computer and converted into joint coordinates; $T = 0$ and $\mathcal{C} = \frac{1}{2}\mathcal{J}$ were also set during this test.

In a first experiment the tip of the soldering iron was heated to 100°C, and the finger was commanded to approach the tip moving from its "initialization" position. The signals detected during finger motion by those elements of the epidermal and dermal sensing layers closest to the soldering tip are shown in Fig. 22A.

The epidermal sensor signal increases rapidly until it reaches a preset threshold value. At this point the

Fig. 22. Signals detected during APPROACH for the finger approaching a hot object (A) and touching a sharp object (B).

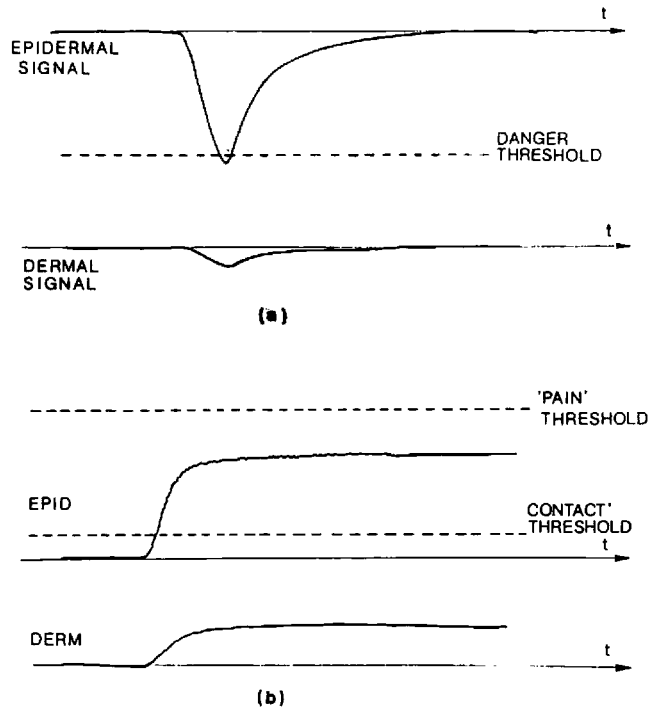

"instinct" algorithm commands the finger to stop its motion and to move back to the initial position. During a typical test the finger, moving at a speed of about 2 cm/s, was able to stop at a distance of about 5 mm from the hot tip, after having covered about 2 mm from the instant the threshold was exceeded.

The response of the epidermal sensor was extremely fast, but the dermal sensing elements, shielded by the upper layers, detected only a negligible pyroelectric signal.

During a second set of experiments the same relatively sharp tip was not heated. In this case no proximity signal was measured by the fingertip sensors. A possible dangerous situation was related to the amplitude of the piezoelectric signals detected by the sensors when the fingertip pressed the tip of the soldering iron.

Piezoelectric signals have a sign opposite to pyroelectric signals. Appropriate thresholds were set for the case of contact sensing. A first threshold was set on the epidermal signal; when the signal generated by one of the epidermal sensing sites exceeded a low-level threshold, the controller inferred that the finger was

Fig. 23. The exploratory trajectory adopted in SHAPE (A) and the reconstructed surface (B).

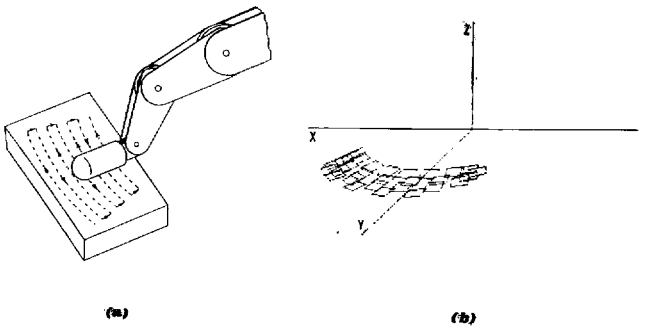

Fig. 24. Flowchart of the program that implements SHAPE and TEXTURE.

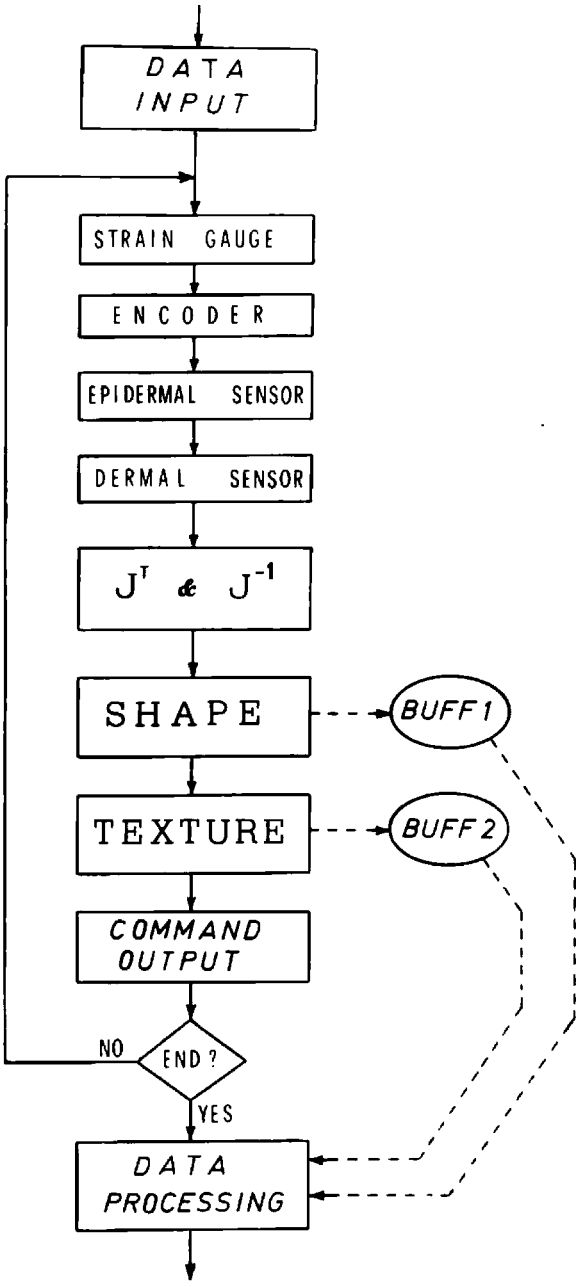

touching something. A second ("pain") threshold on the epidermal signal set the limit at which the "danger" instruction was sent to stop finger motion.

Experimental results illustrating the signals generated by epidermal and dermal sensors when the fingertip touched the soldering iron are shown in Fig. 22B.

Three conditions should be simultaneously verified in order that the "instinct" algorithm sends the O.K. message: The first "contact" threshold must be exceeded, the pain threshold must not be exceeded, and the first derivative of the signal must be zero.

5.2. SHAPE

The present version of the fingertip tactile sensor has a spatial resolution insufficient to allow it to explore complex shapes. A second version, already tested, does not have this limitation (Buttazzo et al. 1986).

In the experiments reported here, SHAPE, a fundamental subroutine that is the basis of the proposed exploratory sequence, was tested by commanding the finger to map only simple surfaces.

A first test was performed by commanding the finger to follow a smooth planar surface (the actual surface was covered with a paper sheet; friction effects between the Mylar coated fingertip sensor and the paper were negligible). See the scheme of Fig. 17: The overall trajectory of the finger was imposed through θ; L was set to be 5 mm, and $F = 1$ N. The finger traced the trajectory sketched in Fig. 23A.

A graphic three-dimensional representation of finger trajectory (and, correspondingly, of object shape) was obtained by an algorithm that draws small square areas having side length proportional to L, orientation corresponding to t, and position corresponding to P. An example of such a representation for a flat surface is given in Fig. 23B.

Fig. 25. Contact locations and orientations recorded by the finger while exploring a curved pipe.

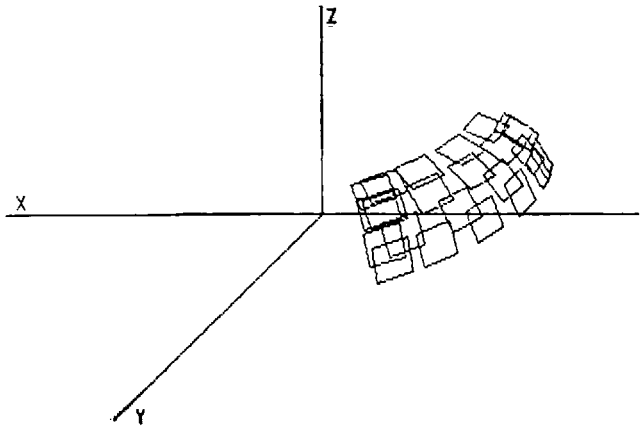

Fig. 26. Signal detected by an epidermal sensing element when the finger rubs the same grooved and curved pipe as in Fig. 25.

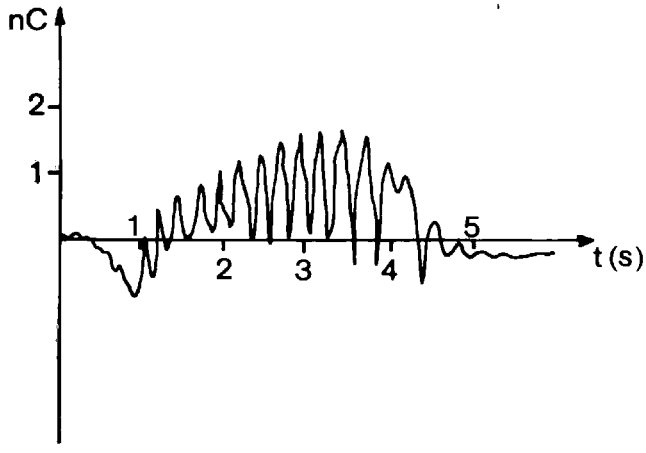

A further test involved the exploration of a plastic pipe (O.D. 50 mm) with grooves (about 3 mm wide and 1 mm deep) on its outer surface. The exploration of this type of object demonstrated the possibility of performing simultaneously different tactile subroutines: The information to extract involves both the overall shape of the pipe and the details of its surface ("texture").

This experiment is described in the next section.

5.3. TEXTURE

A block diagram of the program used to explore the grooved pipe is shown in Fig. 24. The program actually incorporates both SHAPE and TEXTURE. The execution of both subroutines is based on the signal provided by the dermal sensors.

During this test, input data were $L = 10$ mm, $F = 1$ N, and θ was set to allow the finger to explore the pipe. The result of such an exploration is graphed in Fig. 25.

During the execution of TEXTURE, the attention of the high-level controller was focused on the signal detected by the epidermal sensor. Because we have not yet developed special processing algorithms for this signal, the output of the epidermal sensors in contact with the pipe was sent to a charge amplifier and visualized on an oscilloscope.

An example of a signal detected by the epidermal sensor is shown in Fig. 26. The sensor signal shows a number of peaks corresponding exactly to the total number of grooves crossed by the finger. The distance between contiguous peaks is not the same because finger velocity varied from zero to a maximum and back to zero; furthermore, the artifacts around start and stop positions and the variation of peak intensity and of signal level can be attributed to shocks and irregularities during finger motion. Further signal processing (i.e., highpass filtering) is expected to reduce the influence of those artifacts.

5.4. HARDNESS

As already mentioned, measuring a figure of merit of the elastic modulus of the material of which an object is made requires pressing the fingertip tactile sensor on the object and calculating the ratio between the dermal and epidermal sensor signals. The epidermal sensor is predominantly sensitive to strain, whereas the dermal sensor essentially measures stress. Hence, if sample objects of the same dimensions but different compliant materials are pressed by the finger with the same "torque law," the ratio between the two signals is proportional to the slope of the stress–strain relationship of the material.

We prepared four identical object samples shaped as

Fig. 27. Experimental results obtained with HARDNESS. (A) Foam with elastic modulus E = 10^4 *Pa (EPID/DERM = 4.9); (B) rubber with* E = 10^5 *Pa (EPID/DERM = 18.2); (C) rubber with* E = 10^6 *Pa (EPID/DERM = 47.5); (D) rubber with* E = 10^7 *Pa (EPID/DERM = 68.3).*

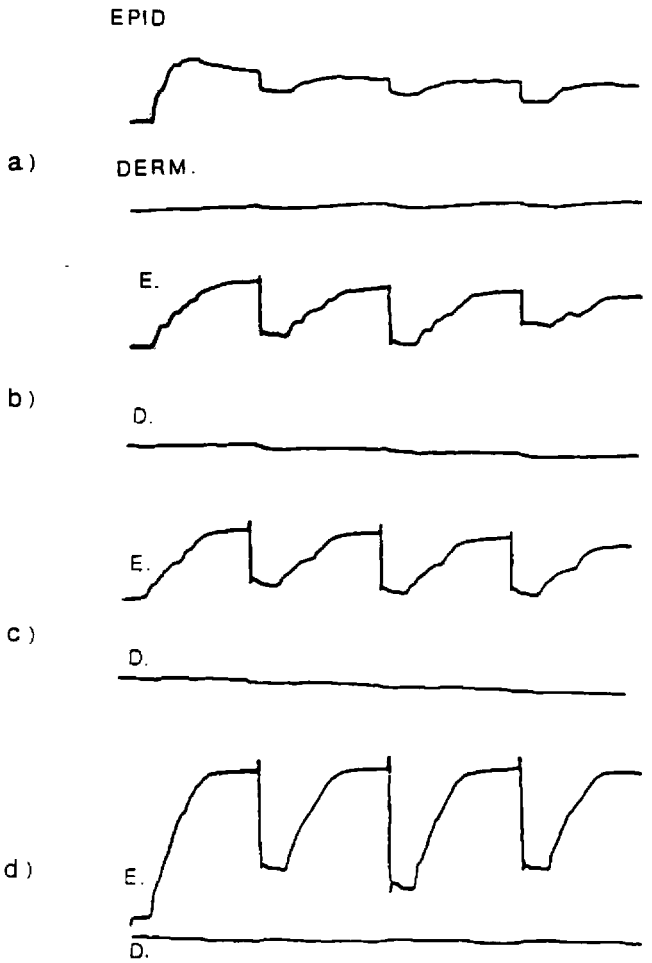

Fig. 28. Signal detected by the epidermal sensor when the finger touches different sample objects and the resistive layer is heated at a temperature of 38°C.

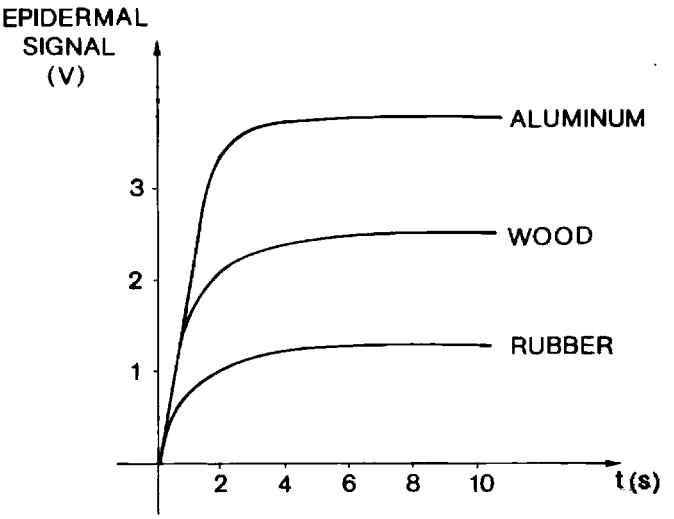

This experiment demonstrates the ability of the subroutine to classify with reasonable specificity the four different object samples on the basis of their moduli of elasticity. Repeatability was also tested and proved to be excellent.

Saturation effects occurred for materials with moduli of elasticity larger than 10^7 Pa and lower than 10^4 Pa.

parallelepipeds, using different rubber materials whose moduli of elasticity fell between 10^4 Pa and 10^7 Pa. Sample thickness was 5 mm for all the samples.

During the experiments the finger was commanded to press each sample with a sinusoidal torque law (frequency 1 Hz; offset force 5 N; peak-to-peak force amplitude 6 N). Examples of experimental signals are shown in Fig. 27, whose caption reports values of the ratio between the amplitude of the epidermal and dermal sensor signals.

In this experiment the dither vibration was not superimposed to the command signal, because signal waveform is not important. Thus the resulting waveform was distorted by friction effects.

5.5. THERMAL

The ability of the finger and of its controller to identify different materials on the basis of their thermal properties was tested with an experimental procedure during which the fingertip pressed the sample object with a force of 5 N (the higher the contact force, the better the thermal contact between object and sensor). After good thermal contact was established, a signal was sent by the computer to a programmable power supply in order to heat the resistive graphite layer incorporated in the fingertip tactile sensor. A calibration procedure permitted the correlation of the temperature of the resistive layer with the electrical and time parameters of the heating pulse. Therefore it was possible, during these preliminary experiments, to operate the heating layer in open-loop conditions.

In this ideal experimental situation (intimate object–sensor thermal contact, identical shape and thickness of the sample object, flat object surface, no finger movement), the amplitude of the pyroelectric signal generated by the epidermal sensor depends only on the thermal properties of the material.

Examples of experimental signals detected for some different materials are shown in Fig. 28.

6. Conclusion

In this paper we have proposed an approach to the study of artificial tactile perception based on the attempt of mimicking sensory motor paradigms typical of humans. Some departures are unavoidable, however, with a single-finger, simplified schematization of human exploratory strategies, the most criticizable being perhaps to have completely separated prehensile from perceptual functions.

The primary aim of this simplification was to reduce theoretical and practical problems associated with the control of a multifingered hand, which would have distracted a significant amount of attention from our real goal of understanding the basic modalities of tactile perception. The extension of the present study to the case of a dexterous hand is actually left to future investigation.

Despite the limitations of this work, results seem to confirm the intuition that a sophisticated, skinlike tactile sensor has a fundamental role in tactile perception. However, our study emphasizes also the less intuitive, but also fundamental, importance of designing a system comprising a dexterous manipulator and a multilevel controller to exploit the sensory capabilities of such a tactile sensor.

In this context the concepts of a single, anthropomorphic finger and of an exploratory strategy based on the decomposition of the complex human tactile perceptual activity in a sequence of elementary sensory motor acts seem to have the potential to provide intriguing opportunities for further investigation in the field.

Acknowledgments

Discussions with Prof. Ruzena Bajcsy at the University of Pennsylvania were extremely helpful.

The authors wish to acknowledge the contribution of A. Bicchi in the design of the robot finger and of the hybrid control, and to thank R. Di Leonardo, R. Francesconi, and F. Vivaldi for their technical help.

Appendix I

The descriptive function D allows us to incorporate the effects of friction into a single nonlinear block of the scheme (Fig. 14) that describes the finger device.

The nonlinear effects introduced by the friction between cables and conduits can be represented as in Fig. 29A, where T_M is the motor torque and f is the friction force (A_1 = value of the maximum static friction force ($f_{S\max}$); A_2 = value of the dynamic friction force (f_d); $B = A_1 - A_2$).

Figure 29B illustrates how a sinusoidal waveform (upper trace) is distorted by the above nonlinearity (lower trace).

From Fig. 29 the following relations can be easily derived:

$$\omega_0(t_1) = \arcsin(A_1/x),$$
$$\omega_0(t_2) = \pi - \arcsin(A_2/x).$$

The function D then becomes

$$D = \frac{(b_1 + ja_1)}{x},$$

where

$$b_1 = \frac{2}{\pi}\int_0^{\pi} y(t)\sin \omega t \, d(\omega t),$$

$$a_1 = \frac{2}{\pi}\int_0^{\pi} y(t)\cos \omega t \, d(\omega t).$$

Fig. 29. Simplified model of the nonlinearity introduced by friction forces in the cable-and-sheath power transmission system (A). Those friction effects distort a sinusoidal waveform (B, upper trace) of amplitude x, as shown in B (lower trace).

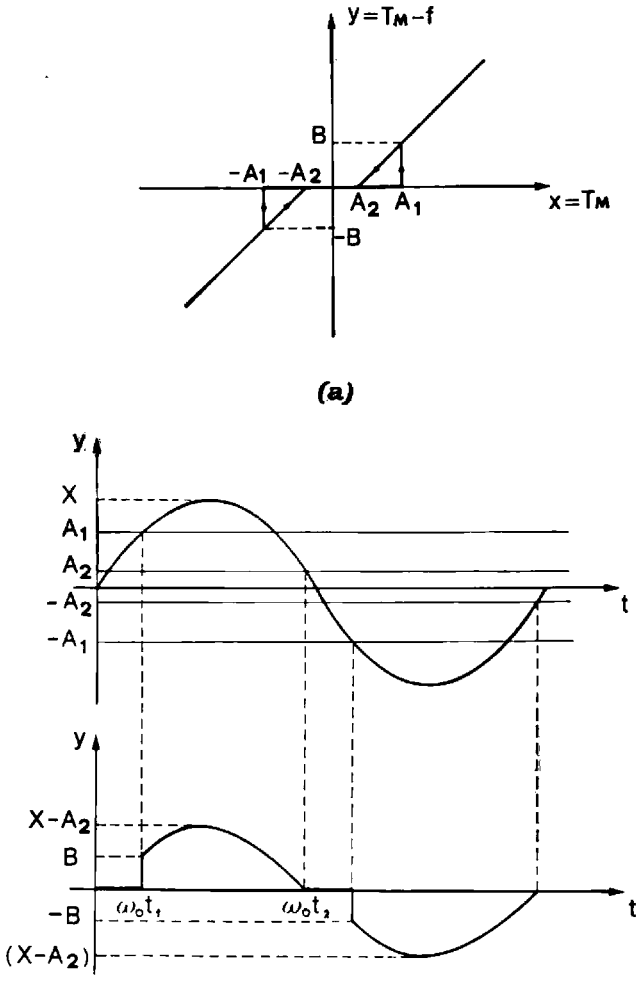

Fig. 30. Nyquist diagram of $-1/D(X)$ calculated for $A_1/f_{s_{max}} = 1$; $A_2/f_{s_{max}} = 0.5$.

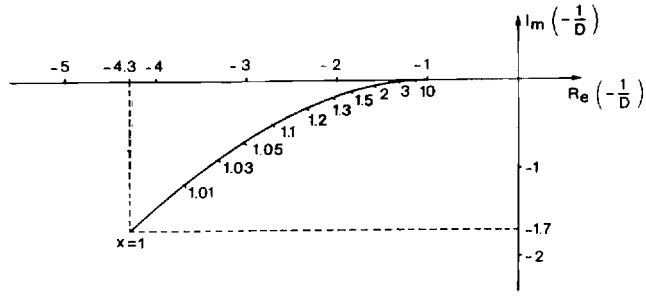

By simple calculations we obtain

$$b_1 = \frac{2}{\pi}\int_{\omega t_1}^{\omega t_2} (x \sin \omega t - A_2) \sin \omega t \, d(\omega t),$$

$$a_1 = \frac{2}{\pi}\int_{\omega t_1}^{\omega t_2} (x \sin \omega t - A_2) \cos \omega t \, d(\omega t),$$

$$\begin{cases} b_1 = \dfrac{x}{\pi}\left[\pi - \varphi_2 - \varphi_1 + \dfrac{A_2}{x}\alpha_2 + \dfrac{A_1}{x}\alpha_1\right] \\ \qquad - 2\dfrac{A_2}{\pi}(\alpha_2 + \alpha_1), \\ a_1 = \dfrac{x}{\pi}\left[\left(\dfrac{A_2}{x}\right)^2 - \left(\dfrac{A_1}{x}\right)^2\right] - 2\dfrac{A_2}{x}\left[\dfrac{A_2}{x} - \dfrac{A_1}{x}\right] \\ \qquad = -\dfrac{(A_2 - A_1)^2}{\pi x}, \end{cases}$$

where

$$\varphi_1 \triangleq \arcsin(A_1/x), \qquad \alpha_1 \triangleq \sqrt{1 - (A_1/x)^2},$$
$$\varphi_2 \triangleq \arcsin(A_2/x), \qquad \alpha_2 \triangleq \sqrt{1 - (A_2/x)^2},$$

and the descriptive function is

$$\mathrm{Re}\{D\} = 1 - \frac{\varphi_1 + \varphi_2}{\pi} + A_1\alpha_1 + A_2\alpha_2 - 2A_2(\alpha_1 + \alpha_2),$$

$$\mathrm{Im}\{D\} = -\frac{(A_2 - A_1)^2}{\pi x^2} = -\frac{1}{\pi}\left(\frac{B}{x}\right)^2.$$

Finally, Fig. 30 shows the Nyquist diagram of $-1/D(x)$, which is necessary for the study of the existence of limit cycles in the finger system.

Appendix II

Based on dermal sensor signals, the coordinate transformation unit (C.T.U.) calculates the following vectors:

n: normal vector to the fingertip surface in the contact point (in the fingertip space).
t: tangent vector to the fingertip surface in the contact point (along a direction specified by the high-level controller), also referred to the fingertip space.
P: contact point coordinates in the absolute frame.

In the fingertip frame coordinates we obtain, for our sensor configuration,

$$t_\theta = \begin{pmatrix} \cos\alpha\cos\theta \\ \sin\theta \\ -\sin\alpha\cos\theta \\ 0 \end{pmatrix}, \qquad P = \begin{pmatrix} R\sin\alpha \\ \delta \\ R\cos\alpha \\ 1 \end{pmatrix},$$

$$n = \begin{pmatrix} \sin\alpha \\ 0 \\ \cos\alpha \\ 0 \end{pmatrix},$$

where, according to Fig. 31, α and δ are parameters that define the active sensor, θ is the step direction, and R is the fingertip radius.

To calculate the coordinates of P in the absolute frame, the C.T.U. uses a homogeneous transformation matrix, which for our finger is

$$\mathcal{T} = \begin{pmatrix} -S_1S_{234} & S_1C_{234} & C_1 & S_1(L_1 + L_2C_2 + L_3C_{23}) \\ -C_1S_{234} & C_1C_{234} & -S_1 & C_1(L_1 + L_2C_2 + L_3C_{23}) \\ -C_{234} & -S_{234} & 0 & -(L_2S_2 + L_3S_{23}) \\ 0 & 0 & 0 & 1 \end{pmatrix},$$

where

L_i = length of the ith link,
$S_j(C_j)$ = sine (cosine) of the jth joint angle,
$S_{jk(l)}$ = sine of the sum of jth and kth (and lth) joint angles.

Consequently, the coordinates of P are

$$P = \begin{pmatrix} S_1\beta + C_1R\cos\alpha \\ C_1\beta - S_1R\cos\alpha \\ -\gamma \\ 1 \end{pmatrix},$$

Fig. 31. Scheme of the finger with its coordinate frame.

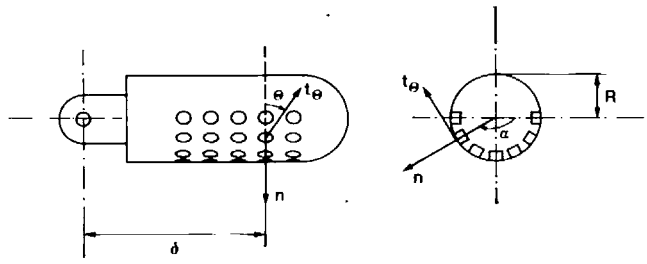

where

$$\beta = \delta C_{234} - S_{234}R\sin\alpha + L_1 + L_2C_2 + L_3C_{23},$$
$$\gamma = \delta S_{23} + C_{234}R\sin\alpha + L_2S_2 + L_3S_{23}.$$

The normal and tangent vectors in the fingertip space are converted, by application of the transpose and inverse Jacobian matrices, into joint torques (T_i) and angular displacements (dQ_i), respectively.

For our device these matrices are

$$J^T = \begin{pmatrix} 0 & 0 & F & 0 \\ A & C & 0 & 1 \\ B & D & 0 & 1 \\ 0 & 0 & 0 & 1 \end{pmatrix},$$

$$J^{-1} = \frac{1}{W}\begin{pmatrix} 0 & 0 & W/F & 0 \\ D & -B & 0 & 0 \\ -C & A & 0 & 0 \\ C-D & B-A & 0 & W \end{pmatrix},$$

where

$$A = L_2C_{34} + L_3C_4,$$
$$B = L_3C_4,$$
$$C = L_2S_{34} + L_3S_4,$$
$$D = L_3S_4,$$
$$F = L_1 + L_2C_2 + L_3C_{23},$$
$$W = AD - BC.$$

The matrix notation used in the block diagram of SHAPE can be developed to obtain the following expressions for joint torques (T_i) and angular displacements (dQ_i):

$$T_1 = K(F + \delta C_{234})\cos\alpha,$$
$$T_2 = K(C + \delta)\sin\alpha,$$

$$T_3 = K(D + \delta) \sin \alpha,$$
$$T_4 = K\delta \sin \alpha,$$
$$dQ_1 = -(h/F) \sin \alpha \cos \theta,$$
$$dQ_2 = (h/W)(D \sin \theta - B \cos \alpha \cos \theta),$$
$$dQ_3 = -(h/W)(C \sin \theta - A \cos \alpha \cos \theta),$$
$$dQ_4 = (h/W)[(C - D) \sin \theta + (B - A) \cos \alpha \cos \theta],$$

where K and h are the imposed normal force and the length of exploratory step, respectively.

References

Abramowitz, D., Goodenow, J., and Paul, B. 1983 (Chicago, Ill.). PAMH (Pennsylvania articulated mechanical hand). *Proc. ASME Conf. on Robotics.*

Albus, J. S. 1981. *Brains, behavior, and robotics.* Peterborough: Byte Books/McGraw-Hill.

Bajcsy, R. 1984. What can we learn from one finger experiments? In *Robotics research,* eds. M. Brady and R. Paul, pp. 509–527. Cambridge: MIT Press.

Bardelli, R., Dario, P., De Rossi, D., and Pinotti, P. C. 1983 (Chicago, Ill.). Piezo and pyroelectric polymers skin-like tactile sensors for robots and prostheses. *Proc. 13th ISIR/Robots 7.*

Basta, F. 1985. Progetto, costruzione e sperimentazione di piattaforma sensorizzata per analisi biomeccaniche. Doctor's Degree Thesis, Department of Engineering, University of Pisa.

Bicchi, A. 1984. Ricerca teorica e sperimentale riguardante sistemi di riconoscimento di parti meccaniche basate su sensori tattili a polimero piezoelettrico: sviluppo di un dispositivo sensorizzato di esplorazione. Doctor's Degree Thesis, Department of Engineering, University of Pisa.

Bicchi, A., Dario, P., and Pinotti, P. C. 1985 (Barcelona, Spain). On the control of a sensorized artificial finger for tactile exploration of objects. *Proc. '85 IFAC Symp. on Robot Control.*

Bridgestone ACFAS Robot System. 1985. Rubbertuators and applications for robots. Technical information. Tokyo, Japan: Bridgestone Co.

Brock, D., and Chiu, S. 1985 (Miami, Fla.). Environment perception of an articulated robot hand using contact sensors. *Proc. ASME Winter Annual Meeting.*

Buttazzo, G., Dario, P., and Bajcsy, R. 1986 (Cambridge, Mass.). Finger based explorations. *Proc. SPIE Symp. on Advances in Intelligent Robotics Systems.*

Dario, P., De Rossi, D., Domenici, C., and Francesconi, R. 1984a (Atlanta, Ga.). Ferroelectric polymer tactile sensors with anthropomorphic features. *Proc. 1st IEEE Int. Conf. on Robotics.*

Dario, P., De Rossi, D., Giannotti, C., Vivaldi, F., and Pinotti, P. C. 1984b. Ferroelectric polymer tactile sensors for prostheses. *Ferroelectrics* 60(1–4):199–214.

Dario, P., Bicchi, A., Vivaldi, F., and Pinotti, P. C. 1985 (St. Louis, Mo.). Tendon actuated exploratory finger with polymeric, skin-like tactile sensor. *Proc. 1985 IEEE Int. Conf. on Robotics and Automation.*

Dario, P., and De Rossi, D. 1985. Tactile sensors and the gripping challenge. *IEEE Spectrum* 22(8):46–52.

Dario, P., Bicchi, A., Fiorillo, A., Buttazzo, G., and Francesconi, R. 1986. A sensorized scenario for basic investigation on active touch. In *Robot sensors,* Vol. 2, *tactile and non-vision,* ed. A. Pugh, pp. 237–245. Kempston, U.K.: IFS and New York: Springer-Verlag.

Goldwasser, S. 1984 (Atlanta, Ga.). Computer architecture for grasping. *Proc. 1st IEEE Int. Conf. on Robotics.*

Harmon, L. D. 1982. Automated tactile sensing. *Int. J. Robotics Res.* 1(2):3–32.

Hillis, W. D. 1981. Active touch sensing. MIT AI Memo AIM-629, Cambridge, Mass.

Jacobsen, S., Wood, J., Knutti, D. F., and Biggers, K. B. 1984a. The UTAH/MIT dexterous hand: Work in progress. *Int. J. Robotics Res.* 3(4):21–50.

Jacobsen, S. C., Knutti, D. F., Biggers, K. B., Iversen, E. K., and Wood, J. E. 1984b (Udine, Italy). An electropneumatic actuation system for the UTAH/MIT dexterous hand. *Proc. 5th CISM-IFToMM Symp. on Theory and Practice of Robots and Manipulators.*

Jacobsen, S. C., Iversen, E. K., Knutti, D. F., Johnson, R. T., and Biggers, K. B. 1986 (San Francisco, Calif.). Design of the UTAH/MIT dexterous hand. *Proc. 1986 IEEE Int. Conf. on Robotics and Automation.*

Kapandji, I. A. 1970. *The physiology of the joints: upper limb,* Vol. 1. London: E. & S. Liverstone.

Khatib, O. 1985 (Tokyo, Japan). The operational space formulation in robot manipulation control. *Proc. 15th ISIR.*

Kriegman, D. J., Siegel, D. M., Narasimhan, S., Hollerbach, J. M., and Gerpheide, G. E. 1985 (St. Louis, Mo.). Computational architecture for the UTAH/MIT hand. *Proc. 1985 IEEE Int. Conf. on Robotics and Automation.*

Nakano, Y., Fujie, M., and Hosada, Y. 1984. Hitachi's robot hand. *Robotics Age* 6(7):18–20.

Okada, T., and Tsuchiya, S. 1977 (Tokyo, Japan). On a versatile finger system. *Proc. 7th ISIR.*

Patterson, R. W., and Nevill, G. E. 1986. Performance of an induced vibration touch-sensor. In *Robot sensors,* Vol. 2,

tactile and non-vision, ed. A. Pugh, pp. 219–228. Kempston, U.K.: IFS and New York: Springer-Verlag.

Paul, R. P. 1981. *Robot manipulators: mathematics, programming and control.* Cambridge: MIT Press.

Phillips, J. R., and Johnson, K. O. 1981. Tactile spatial resolution. II: Neural representation of bars, edges and gratings in monkey primary afferents. *J. Neurophysiol.* 46(6):1192–1203.

Raibert, M. H., and Craig, J. J. 1981. Hybrid position-force control of robot manipulators. *J. Dyn. Syst. Meas. Contr.* 102:126–133.

Russell, R. A. 1985. A thermal sensor array to provide tactile feedback for robots. *Int. J. Robotics Res.* 4(3):35–39.

Salisbury, J. K. 1980 (Albuquerque, N.M.). Active stiffness control of a manipulator in cartesian coordinates. *Proc. IEEE Conf. Decision and Control.*

Salisbury, J. K., and Craig, J. J. 1982. Articulated hands: Force control and kinematic issues. *Int. J. Robotics Res.* 1(1):4–17.

Salisbury, J. K. 1984a (Tokyo, Japan). Design and control of an articulated hand. *Int. Symp. on Design and Synthesis.*

Salisbury, J. K. 1984b. Interpretation of contact geometries from force measurements. In *Robotics research,* eds. M. Brady and R. Paul, pp. 565–577. Cambridge: MIT Press.

Sessler, G. M. 1981. Piezoelectricity in polyvinylidene fluoride. *J. Acoust. Soc. Am.* 70(6):1596–1608.

Shimano, B. 1978. The kinematic design and force control of computer-controlled manipulators. Ph.D. Thesis, Stanford University.

Siegel, D. M., Garabieta, I., and Hollerbach, J. M. 1986 (San Francisco, Calif.). An integrated tactile and thermal sensor. *Proc. 1986 IEEE Int. Conf. on Robotics and Automation.*

Turing, A. M. 1950. Computing machinery and intelligence. *Mind* 59:433–460.

Wu, C. H. 1985. Compliance control of a robot manipulator based on joint torque servo. *Int. J. Robotics Res.* 4(3):55–71.

Zhang, H., and Paul, R. P. 1985 (St. Louis, Mo.). Hybrid control of robot manipulators. *Proc. 1985 IEEE Int. Conf. on Robotics and Automation.*